

Association of Uranium with Iron Oxides Typically Formed on Corroding Steel Surfaces

C. J. DODGE,*† A. J. FRANCIS,†
J. B. GILLOW,† G. P. HALADA,‡
C. ENG,‡ AND C. R. CLAYTON‡

Environmental Sciences Department, Brookhaven National Laboratory, Upton, New York 11973, and Department of Materials Science and Engineering, SUNY at Stony Brook, Stony Brook, New York 11794-2275

Decontamination of metal surfaces contaminated with low levels of radionuclides is a major concern at Department of Energy facilities. The development of an environmentally friendly and cost-effective decontamination process requires an understanding of their association with the corroding surfaces. We investigated the association of uranium with the amorphous and crystalline forms of iron oxides commonly formed on corroding steel surfaces. Uranium was incorporated with the oxide by addition during the formation of ferrihydrite, goethite, green rust II, lepidocrocite, maghemite, and magnetite. X-ray diffraction confirmed the mineralogical form of the oxide. EXAFS analysis at the U L_{III} edge showed that uranium was present in hexavalent form as a uranyl oxyhydroxide species with goethite, maghemite, and magnetite and as a bidentate inner-sphere complex with ferrihydrite and lepidocrocite. Iron was present in the ferric form with ferrihydrite, goethite, lepidocrocite, and maghemite; whereas with magnetite and green rust II, both ferrous and ferric forms were present with characteristic ferrous:total iron ratios of 0.65 and 0.73, respectively. In the presence of the uranyl ion, green rust II was converted to magnetite with concomitant reduction of uranium to its tetravalent form. The rate and extent of uranium dissolution in dilute HCl depended on its association with the oxide: uranium present as oxyhydroxide species underwent rapid dissolution followed by a slow dissolution of iron; whereas uranium present as an inner-sphere complex with iron resulted in concomitant dissolution of the uranium and iron.

Introduction

The Department of Energy possesses about 1 million metric ton of radioactively contaminated steels and other metals. The decontamination of these materials at its nuclear processing facilities is receiving increased attention because most of it is only slightly contaminated or "suspect" (1). The development of a safe, cost-effective decontamination methodology for recycling these materials depends on a fundamental understanding of the association of radionuclides with iron oxides formed on corroding steel surfaces.

The iron oxide coating formed on steel surfaces is influenced by the type of steel as well as by environmental

factors, including oxygen, moisture, the presence of other ions, and the E_h and pH of the local environment (2). The oxides found on corroding steel surfaces include ferrihydrite, goethite, green rusts, hematite, lepidocrocite, maghemite, and magnetite (3–6). Wolski (3) identified the presence of an ordered maghemite on iron couplers buried in the soil for extended periods. McGill et al. (4) concluded that a stable green rust formed on cast-iron pipes was structurally different from that of green rust II (GR II). Magnetite and lepidocrocite also were identified. Music et al. (5) identified a mixture of lepidocrocite, magnetite, and an amorphous oxide from low-carbon steel in aqueous solutions at 20 °C; however, at 120 °C, magnetite was the dominant component with some ferrihydrite. Misawa et al. (6) observed that, in a neutral or slightly acidic environment, lepidocrocite was the predominant rust, whereas under more acidic conditions, goethite formation was favored.

Iron oxides have been shown to play an important role in the retention of uranium. Gabriel et al. (7) showed that the adsorption of uranium onto sand coated with synthetic goethite occurred with the release of protons from low- and high-affinity binding sites. The conversion of iron oxides to more stable forms has been shown to affect its ability to immobilize uranium. Sato et al. (8) reported that goethite, hematite, and ferrihydrite present on the surfaces of iron nodules scavenged uranium from groundwater downgradient of a uranium ore deposit. The aging of the surface oxide resulted in the stabilization of the adsorbed uranium. Quantitative coprecipitation of uranium with 2-line ferrihydrite was reported by Bruno et al. (9). However, the subsequent transformation to crystalline hematite and goethite resulted in less sorption capacity for uranium than the freshly prepared ferrihydrite.

The association of uranium with well-characterized or aged iron oxides has been studied to a limited extent. EXAFS analysis has shown that uranium added to ferrihydrite at pH 6.0 formed an inner-sphere, bidentate complex with the oxide surface (10). Moyes et al. (11) showed that uranium was associated with goethite and lepidocrocite through equatorial coordination of two surface oxygens from an iron octahedron. EXAFS and electrophoretic measurements revealed that uranium adsorption to hematite surfaces at pH > 4.5 occurred with the formation of a dimeric hematite–U(VI)–carbonato complex (12).

Although structural information on the association of uranium with a few oxides has been determined, little is known of the uranium association with oxides commonly found on corroding surfaces. In this study, we determined the molecular association of uranium during iron oxide formation, thereby simulating the corrosion process.

Materials and Methods

Preparation of Oxides with Uranium. *Ferrihydrite* ($Fe_2O_3 \cdot H_2O$) with U. Ferrihydrite was synthesized according to the method of Raven et al. (13). A solution containing 0.2 M ferric nitrate nonahydrate (Sigma, MO) and 10 mM uranyl nitrate hexahydrate (BDH Chemicals Ltd., Poole, England) was adjusted to pH 7.5 by adding 1 M KOH at a fixed rate of approximately 20 mL/min while vigorously stirring. Once the pH stabilized, the suspension was washed three times with 0.1 M NaCl, and the solid was collected after centrifugation at 3000g for 10 min. The sample was dried overnight at 60 °C.

Goethite (α - $FeOOH$) with U. Goethite was synthesized according to Atkinson et al. (14). A solution of 0.1 M ferric nitrate nonahydrate and 5 mM uranyl nitrate hexahydrate

* Corresponding author telephone: (631)344-7234; fax: (631)344-7303; e-mail: dodge1@bnl.gov.

† Brookhaven National Laboratory.

‡ SUNY at Stony Brook.

was adjusted to pH 12, and the precipitate was aged for 24 h at 60 °C. Then, it was washed several times with deionized water and dried overnight at 60 °C.

GR II with U. GR II was synthesized as described by Srinivasan et al. (15) with slight modification. A solution containing 0.2 M ferrous sulfate heptahydrate (Sigma, MO) and 10 mM uranyl nitrate hexahydrate was adjusted to pH 8.2 under a N₂ atmosphere. Filtered oxygen was bubbled through the solution at a rate of 60 mL/min until the pH reached 8.2. The precipitate was collected and stored as a suspension under N₂.

Lepidocrocite (γ -FeOOH) with U. A solution of 60 mM ferrous chloride hexahydrate (Sigma, MO) and 3 mM uranyl nitrate hexahydrate was adjusted to pH 6.8 (16). Compressed air was bubbled through the solution at a rate of 250 mL/min. After the pH stabilized, the product was collected by centrifugation, washed several times with deionized water, and dried overnight at 60 °C.

Maghemite (γ -Fe₂O₃) with U. Maghemite was synthesized by heating magnetite at 250 °C for 5 h (17).

Magnetite (Fe₃O₄) with U. Magnetite was synthesized according to Sidhu et al. (18). A solution containing 0.5 M ferrous sulfate heptahydrate and 25 mM uranyl nitrate hexahydrate was boiled under N₂ gas. A total of 300 mL of a mixture of KNO₃ (0.26 M) and KOH (3.3 M) was added dropwise over 1 h while maintaining a blanket of N₂ gas over it. The suspension then was boiled for an additional 30 min and allowed to cool. The resulting black precipitate was collected by centrifugation, washed several times with deionized water, and finally, washed twice with acetone.

For comparison, we also synthesized these various iron oxides without uranium. All operations with uranium were performed in a HEPA-filtered fume hood. All samples, except for GR II, were dried and pulverized in an agate mortar before characterization.

Uranium Hydroxide [UO₂(OH)₂]. Uranyl hydroxide was prepared by dissolving uranyl nitrate in deionized water and adjusting the pH to 7.0 with NaOH. The precipitate was collected by centrifugation, washed three times with deionized water, dried overnight at 60 °C, and ground to a fine powder.

Chemical Composition of Oxides. Fifty milligrams of the oxide was dissolved in 40 mL of 6 M HCl, in duplicate samples. Total iron and uranium were determined using inductively coupled plasma-atomic emission spectroscopy (ICP-AES). The oxidation states for iron and uranium were determined spectrophotometrically by the *o*-phenanthroline (19) and bromo-PADAP methods (20), respectively.

Exchangeable Iron and Uranium. We determined the readily exchangeable forms of Fe and U with the oxides by adding 40 mL of 1 M MgCl₂ to 20 mg of the oxide containing uranium, in duplicate samples. The samples were placed on a rotary shaker at 150 rpm for 2 h and filtered through a 0.45- μ m filter, and the Fe and U in solution were analyzed by ICP-AES.

Mineralogical Characterization. The mineralogical forms of the oxides with and without uranium were determined by X-ray powder diffraction using a Phillips XRG model 3100 analyzer. Powder spectra were obtained from 5 to 90° 2 θ at a scan rate of 0.02°/s. GR II was vacuum-dried before analysis. The spectra then were compared with reference spectra in the JCPDS International Centre for Diffraction Data library.

Dissolution Profile of Uranium Associated with Oxides. To determine the chemical association of uranium with iron oxide, 40 mL of 6 M HCl was added to 50 mg of the oxide, in duplicate samples. Periodically, (up to 12 h), a 3-mL aliquot was removed, filtered through a 0.45- μ m filter, and analyzed for iron and uranium.

X-ray Absorption Near Edge Structure (XANES). XANES analysis was performed at the U L_{III} edge for each oxide. The

spectra were background-subtracted and normalized to the edge jump. The inflection point for the uranium dioxide absorption edge was set to 17166 eV. The oxidation state of uranium in the samples was determined by comparing the energy position at the inflection point with that of the standards uranium dioxide and uranium trioxide (Atomergic Chemicals, New York).

Extended X-ray Absorption Fine Structure (EXAFS). EXAFS analysis of the oxide at the U L_{III} (17.166 keV) absorption edge was performed on beamline X11A at the National Synchrotron Light Source (NSLS) to determine the association of U with the oxide matrix. This technique provides information on the local three-dimensional environment surrounding the uranium and identifies near-neighbor atoms, interatomic distances, coordination numbers, and geometry. Ten milligrams of the oxide was mixed in an agate mortar with 30 mg of boron nitride, and the sample was placed in a heat-sealed polypropylene bag (0.2 mil). Analysis was performed in the fluorescence mode using an Ar-filled ion chamber and sample beam dimensions of 1.0 mmV \times 10 mmH. Sample scans were collected and averaged (up to 5 scans per sample). Data were analyzed using the UW EXAFS analysis software package. Single shells were isolated from the Fourier transforms, and the data were fitted for atom type, coordination number, atomic distance, and Debye–Waller factor by comparison with the theoretical EXAFS modeling code FEFF7 (21). The amplitude reduction factor was fixed at 0.9, and the energy threshold was allowed to vary. Multiple scattering path for uranyl ion (4-legged O–U–O) was included where necessary. The entire EXAFS function was fitted with four shells.

X-ray Photoelectron Spectroscopy (XPS). XPS measurements were made using a custom-designed spectrometer with a V. G. Scientific (Fisons) CLAM 100 hemispherical analyzer controlled by a VGX900I data acquisition system. An Al K $\alpha_{1,2}$ (1486.6 eV) X-ray source and 20 eV pass energy were used for all analyses providing a fwhm for the Au4f_{7/2} singlet of 1.35 eV. For reference, the binding energy of the Au4f_{7/2} singlet was 83.8 eV and that of the Cu2p_{3/2} singlet was 932.4 eV. All binding energies were corrected for charge shifting by referencing them to the C1s line from adventitious carbon at 284.6 eV. All data were smoothed following the method developed by Savitsky and Golay (22) and modified by Sherwood (23) to cover truncation errors at the end of the spectra. Further details of the curve fitting and data analysis procedure are given elsewhere (24, 25).

Fourier Transform Infrared Spectroscopy (FTIR). FTIR spectra were obtained using a Nicolet 760 infrared spectrometer modified to collect data in both mid- and far-infrared regions. Samples were mixed with potassium bromide (1:10) and ground to a fine powder. Spectra were collected using an MCT-A detector with data resolution set to 2 cm⁻¹ and summed over 256 scans to improve the signal-to-noise ratio. A Gemini sampling accessory (Spectra-Tech) collected diffuse reflectance data from powder samples. A spectral background from potassium bromide (99.5%) was subtracted from each resulting spectrum; the analysis chamber was purged continuously with doubly dried air to prevent the absorption of water vapor, and a global-type IR source was used.

Results

Metal Content of Oxides. Table 1 shows the content of iron and uranium for each oxide with and without uranium. Ferrihydrite, goethite, and lepidocrocite samples without uranium show similar amounts of iron: 9.12 \pm 0.15, 8.95 \pm 0.21, and 8.65 \pm 0.16 mmol g⁻¹ as ferric ion, respectively. Maghemite and magnetite showed greater amounts of Fe (12.8 \pm 0.8 and 13.0 \pm 0.6 mmol g⁻¹ iron, respectively) because of their greater crystallinity and structural similarity. GR II

TABLE 1. Iron and Uranium Content of Iron Oxides

mineral	composition (mmol g ⁻¹) ^a	
	iron	uranium
ferrihydrate (Fe ₂ O ₃ ·H ₂ O)	9.12 ± 0.15	
ferrihydrate + U	7.51 ± 0.14	0.43 ± 0.01
goethite (α-FeOOH)	8.95 ± 0.21	
goethite + U	7.84 ± 0.09	0.43 ± 0.02
green rust II ^b	4.24 ± 0.08	
green rust II + U ^c	3.97 ± 0.10	0.19 ± 0.01
lepidocrocite (γ-FeOOH)	8.65 ± 0.16	
lepidocrocite + U	7.93 ± 0.03	0.54 ± 0
maghemite (γ-Fe ₂ O ₃)	12.8 ± 0.8	
maghemite + U	10.7 ± 0.4	0.54 ± 0.02
magnetite (Fe ₃ O ₄)	13.0 ± 0.6	
magnetite + U	10.5 ± 0.2	0.53 ± 0.01

^a ±1 SEM. ^b Fe(II):total Fe = 0.62 ± 0.02. ^c Fe(II):total Fe = 0.73 ± 0.01.

contained the lowest level of total iron (4.24 ± 0.08 mmol g⁻¹), most probably due to the presence of sulfate ions as well as waters of hydration. Magnetite and GR II contained both ferrous and ferric ions with a ferrous:total iron ratio of 0.65 for magnetite and of 0.73 ± 0.01 for GR II, which is similar to the stoichiometric ratio found in the natural mineral phase.

With the addition of U, the amount of iron decreased stoichiometrically by 10–20% because of its incorporation.

Essentially, all the added U was associated with the oxide: 0.43 ± 0.01 mmol g⁻¹ with ferrihydrate, 0.43 ± 0.02 mmol g⁻¹ with goethite, 0.54 ± 0 mmol g⁻¹ with lepidocrocite, 0.54 ± 0.02 mmol g⁻¹ with maghemite, and 0.53 ± 0.01 mmol g⁻¹ with magnetite. In the presence of uranium, the Fe(II):total iron ratio of GR II was reduced from 0.73 ± 0.01 to 0.62 ± 0.02. No attempt was made to remove adsorbed or structural water from the oxides.

Exchangeable Iron and Uranium. The amount of iron in the exchangeable form varied from 0.01 ± 0 mmol g⁻¹ (0.1%) in the lepidocrocite sample to 0.09 ± 0 (2%) mmol g⁻¹ in the GR II sample (data not shown). The amount of uranium released into solution was not detectable (<0.01 mmol g⁻¹) for any of the oxides tested.

Mineralogical Characterization. Figure 1 presents the X-ray diffraction patterns for iron oxide minerals with and without uranium. Ferrihydrate showed two broad reflections at 35 and 62 2θ° that identify the oxide as 2-line ferrihydrate (16). The identification of goethite, lepidocrocite, maghemite, and magnetite were confirmed by comparison with JCPDS files 29-713, 8-98, 39-1346, and 19-629, respectively. The GR II sample without uranium was compared with JCPDS file 13-90 and showed no match. However, the peaks correspond most closely to the lepidocrocite phase, which probably formed due to oxidation of the sample during its transfer prior to analysis. The maghemite spectrum showed dominant reflections at 35.6, 62.9, and 57.3 2θ°. There is a shift to higher

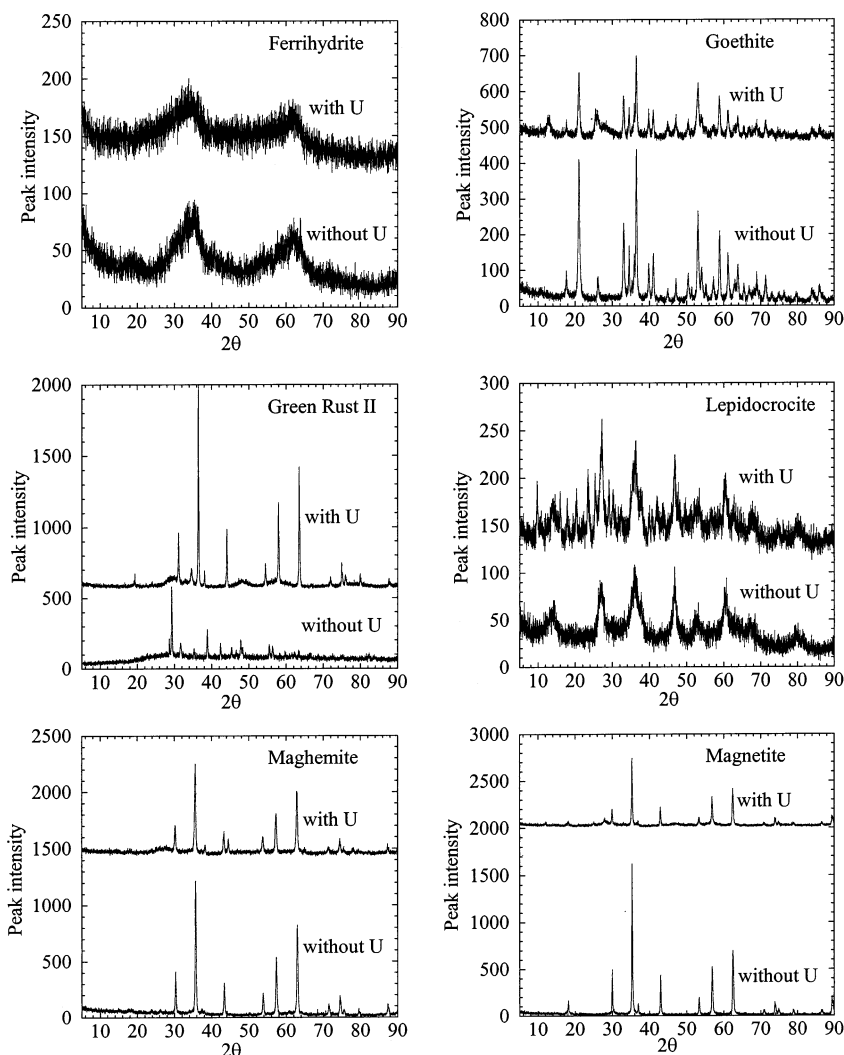


FIGURE 1. X-ray diffraction spectra with and without uranium for ferrihydrate, goethite, green rust II, lepidocrocite, maghemite, and magnetite.

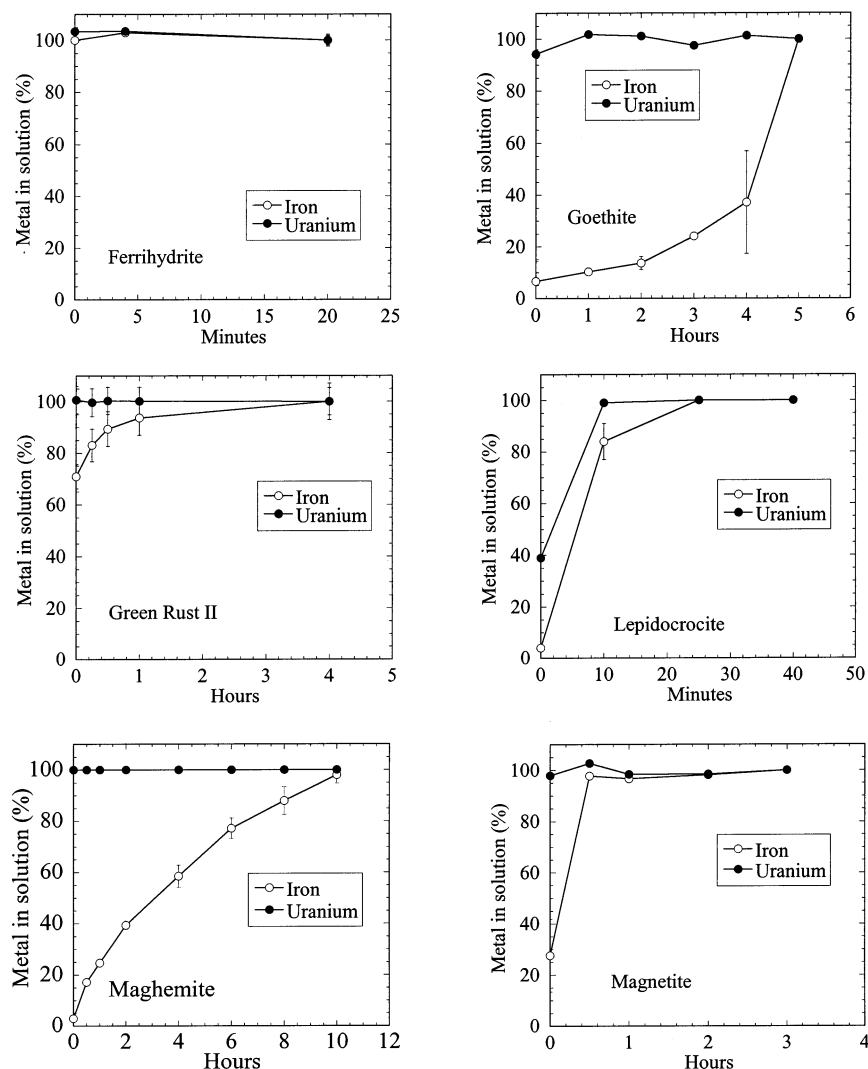


FIGURE 2. Dissolution profile of uranium in 6 M HCl for ferrihydrite, goethite, green rust II, lepidocrocite, maghemite, and magnetite. Error bars are \pm SEM.

2θ by 0.2° in maghemite as compared to magnetite as a result of ferrous ion oxidation to the ferric form.

In the presence of U, peak intensity decreased for ferrihydrite, goethite, magnetite, and maghemite probably because of stoichiometric dilution by uranium and not a change in crystallinity. No shift in peak position was observed for any of the oxides except for GR II, indicating that uranium did not influence the chemical structure of the oxide. Additional peaks were noted at 12 and $28^\circ 2\theta$ for goethite, lepidocrocite, and magnetite indicating the presence of uranyl hydroxide hydrate species (e.g., JCPDS 29-1376; 23-1461). The addition of U during GR II formation converted it to a pure magnetite phase.

Dissolution Profile of Iron Oxides in 6 M HCl. Figure 2 plots the dissolution profiles in 6 M HCl for iron oxides containing U. The rate and extent of Fe and U dissolution varied with the type of oxide. Dissolution of the oxide as measured by Fe in solution was completed in 5 min for ferrihydrite, in 25 min for lepidocrocite, in 30 min for magnetite, in 5 h for goethite and GR II, and in 10 h for maghemite. Uranium dissolution occurred in <5 min for ferrihydrite, <10 min for lepidocrocite, <15 min for GR II, <30 min for maghemite and magnetite, and <1 h for goethite.

EXAFS Analysis. Figure 3A presents the raw k^3 -weighted data (3.2 – 13.5 \AA^{-1}) at the $U_{L_{III}}$ edge for ferrihydrite, goethite, lepidocrocite, maghemite, and magnetite. The oscillations

in the low k region (3.2 – 9.5 \AA^{-1}) are dominated by back-scattering from the nearest-neighbor oxygen atoms in the axial and equatorial planes of uranium. The complex oscillation patterns observed at high k (12 \AA^{-1}) indicate the presence of a large scatterer (Fe, U). The oscillation associated with uranium in ferrihydrite at 7.5 \AA^{-1} is fairly broad and indicative of bidentate oxygen coordination.

Fourier transformed spectra for the oxides, the proposed structures for the uranium, and the corresponding fitting information and proposed structures are found in Figure 3B and Table 2. The peaks in the figure represent a pseudo-radial distribution function for atoms in the near-neighbor region of uranium. The shells are uncorrected for phase shifts ($\Delta R = 0.2$ – 0.5 \AA depending on type of atom). The amplitude of the shells provides information on coordination numbers for similar near-neighbor atoms. We note that in the presence of more than one phase, average atomic information is obtained. The first shell distances are clustered in the range of 1.77 – 1.83 \AA and vary from 2.0 O atoms in magnetite to 2.4 O atoms in ferrihydrite. The second and third shells in each sample exhibit different ranges because of the type of oxygen bonding. Ferrihydrite has one large amplitude peak showing 3.0 equatorial O atoms at 2.35 \AA . Another peak at 2.54 \AA is due to the presence of 2.0 O atoms. The presence of a U–Fe interaction at 3.42 \AA indicates that uranium is bound to iron in bidentate fashion through the two equatorial

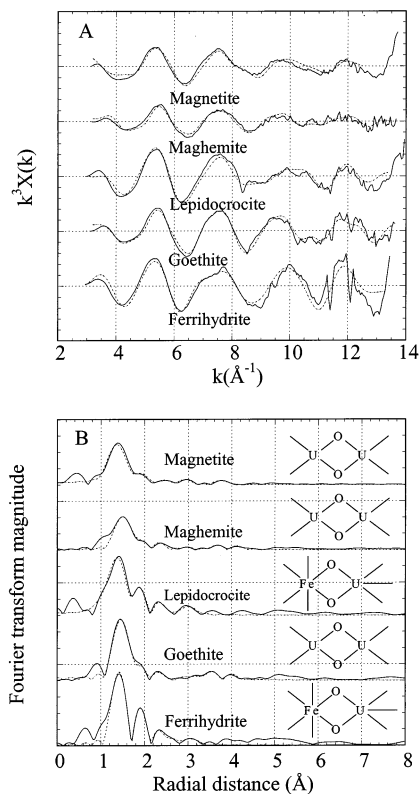


FIGURE 3. EXAFS spectra at the U L_{III} edge showing (A) k^3 -weighted EXAFS spectra (2.9–13.3 Å⁻¹) and (B) Fourier transform showing association of uranium with ferrihydrite, goethite, lepidocrocite, maghemite, and magnetite. Experimental data (—); theoretical fit (---).

TABLE 2. EXAFS Structural Parameters for Uranium Association with Iron Oxides^a

sample	atoms	<i>N</i>	<i>R</i> (Å)	σ^2	<i>F</i>
ferrihydrite	U–O _{ax}	2.4	1.79	0.0011	0.119
	U–O _{eq1}	3.0	2.35	0.0042	
	U–O _{eq2}	2.0	2.54	0.0050	
	U,Fe	1.0	3.42	0.0102	
goethite	U–O _{ax}	2.3	1.82	0.0033	0.062
	U–O _{eq1}	2.8	2.26	0.0035	
	U–O _{eq2}	1.7	2.51	0.0030	
	U,U	1.1	3.71	0.0063	
lepidocrocite	U–O _{ax}	2.3	1.77	0.0031	0.125
	U–O _{eq1}	2.9	2.31	0.0038	
	U–O _{eq2}	2.2	2.54	0.0048	
	U,Fe	1.0	3.44	0.0034	
maghemite	U–O _{ax}	2.2	1.83	0.0050	0.025
	U–O _{eq1}	1.5	2.28	0.0034	
	U–O _{eq2}	2.6	2.55	0.0053	
	U,U	1.0	3.85	0.0066	
magnetite	U–O _{ax}	2.0	1.78	0.0010	0.161
	U–O _{eq1}	1.6	2.26	0.0069	
	U–O _{eq2}	2.5	2.52	0.0050	
	U,U	1.0	3.91	0.0087	

^a Coordination number (*N*), interatomic distance (*R*), disorder parameter (σ^2), and overall goodness-of-fit parameter (*F*).

oxygens at 2.54 Å. Uranium in goethite shows 2.3 axial oxygens at 1.82 Å and a split equatorial oxygen shell containing 2.8 O atoms at 2.26 Å and 1.7 O atoms at 2.51 Å. The uranium in lepidocrocite is bonded to 2.3 axial O atoms at 1.77 Å. The equatorial shell is split, with 2.9 O atoms at 2.31 Å and 2.2 O atoms at 2.54 Å. There is a U–Fe interaction at 3.44 Å.

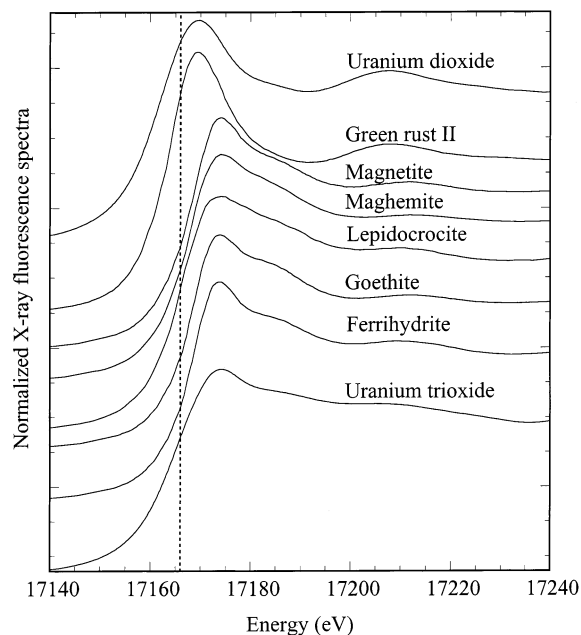


FIGURE 4. XANES spectra showing normalized U L_{III} edges for uranium trioxide, ferrihydrite, goethite, lepidocrocite, maghemite, green rust II, and uranium trioxide. The vertical line at 17166 eV indicates the inflection point for U(IV) species.

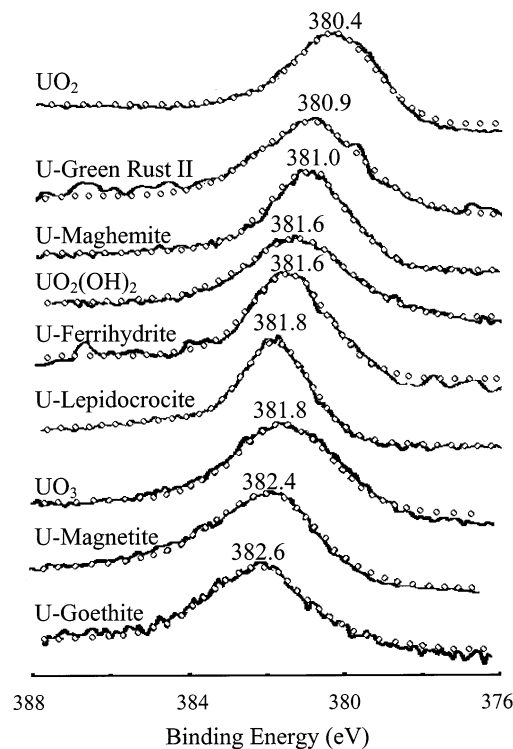


FIGURE 5. X-ray photoelectron spectroscopy (XPS) showing raw (—) and fitted (···) U4f_{7/2} binding energy spectra for ferrihydrite, goethite, green rust II, lepidocrocite, maghemite, magnetite, and UO₂, UO₃, and UO₂(OH)₂ standards.

Uranium in maghemite shows 2.2 axial O atoms at 1.83 Å and equatorial oxygens consisting of 1.5 O atoms at 2.28 Å and 2.6 O atoms at 2.55 Å. A U–U interaction is noted at 3.85 Å. Uranium in magnetite has 2.0 O atoms at 1.78 Å and an equatorial region containing 1.6 O atoms at 2.26 Å and 2.5 O atoms at 2.52 Å. There is a U–U interaction at 3.91 Å. The coordination environment for uranium in maghemite

TABLE 3. Correlation of the Absorption Band Frequency (FTIR) and Axial Oxygen Bond Length (EXAFS) in Uranium Associated with Iron Oxides

sample	absorption band (cm ⁻¹)	U–O bond length (Å)
uranium hydroxide	896	1.81
uranium oxyhydroxides		
goethite	896	1.82
maghemite	905 ^a	1.83
magnetite	907	1.78
U–Fe association		
ferrihydrite	900 ^a	1.79
lepidocrocite	915	1.77
green rust II	920	na ^b

^a Broad peak. ^b na, not applicable.

is similar to magnetite, as expected, since the maghemite coprecipitate was prepared by heating of the magnetite.

XANES Analysis. Figure 4 presents the XANES spectra for ferrihydrite, goethite, GR II, lepidocrocite, maghemite, magnetite, and the standards uranium dioxide and uranium trioxide. The vertical line is set to the absorption edge for the uranous ion at 17166 eV. The shape and position of the XANES spectra for ferrihydrite, goethite, lepidocrocite, maghemite, and magnetite show that uranium is predominantly present in the hexavalent form for these oxides. The spectra also exhibit two multiple scattering (MS) resonances at 20 and 60 eV above the absorption edge that are diagnostic for the uranyl ion. The differences in the XANES structure have been attributed to the chemical environment of the uranyl ion (26). Magnetite and maghemite have similar MS resonances at 43 eV above the absorption edge. However, the MS feature at 16 eV above the absorption edge is broadened in the maghemite. Goethite has a MS resonance at 44 eV above the edge with enhancement of the MS resonance at 16 eV with respect to the maghemite and magnetite. Lepidocrocite and ferrihydrite exhibit a MS resonance at 41 eV, with lepidocrocite showing a broadened MS at 17 eV above the absorption edge. The position of the absorption edge for the GR II sample is shifted to lower energy by 2 eV, identical to the shift observed for uranium dioxide standard, indicating that U is present in the tetravalent form. The absence of an MS peak at 20 eV above the absorption edge is typical for this oxidation state.

XPS Analysis. Figure 5 shows the XPS spectra at the U4f_{7/2} binding energy for uranium standards and ferrihydrite (381.6 eV), lepidocrocite (381.8 eV), maghemite (381.0), and magnetite (382.4 eV). The binding energies for the oxides are very similar to the uranium trioxide standard (381.8 eV) and in the range observed (381.5–382.2 eV) for uranyl species (27). This confirms that uranium in these oxides occurs in the hexavalent state. Goethite shows a peak binding energy at 382.6 eV, higher than that observed for the other oxides. The uranium in GR II exhibited a binding energy of 380.9 eV, similar to that observed for uranium dioxide (380.4 eV), suggesting that uranium is in the tetravalent state. No peak for hexavalent uranium was noted in GR II. Analysis of the sample oxides at the Fe2p binding energy shows the Fe to be bonded primarily to hydroxyl groups and as Fe₂O₃ (data not shown).

FTIR Analysis. Diffuse reflectance spectra (650–1150 cm⁻¹) were obtained for U-containing goethite, lepidocrocite, GR II, maghemite, ferrihydrite, and magnetite (Table 3 and Figure 6). After coprecipitation, FTIR analysis of these samples showed an emergence of a peak in the 900 cm⁻¹ region. The values obtained in this region for each oxide are (cm⁻¹) 896, 915, 920, 905, 900, and 907, respectively. The positions of these peaks are in general agreement with a uranyl hydroxide

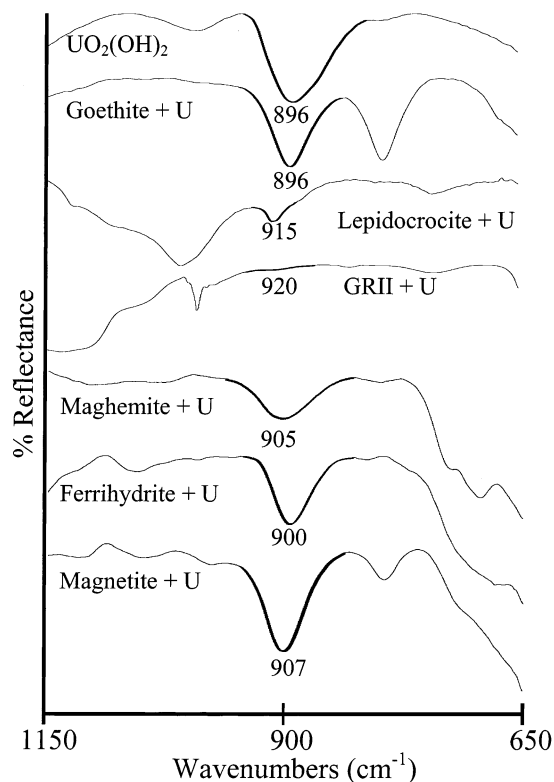


FIGURE 6. Fourier transform infrared absorption spectra for uranyl hydroxide and uranium coprecipitated with goethite, lepidocrocite, green rust II, maghemite, ferrihydrite, and magnetite. The highlighted spectra (896–920 cm⁻¹) show the asymmetric stretching frequencies for uranium.

standard and published values (28). In the uranyl hydroxide standard, the slight shoulder to the right of the peak at 896 cm⁻¹ indicates that the peak may be a combination of a strong O=U=O asymmetric stretching and medium μ -OH bending components. Goethite has characteristic peaks observed at 890 and 790 cm⁻¹, the first of which may coincide with the peak of interest. Additional characteristic peaks for lepidocrocite observed at 1013 and 742 cm⁻¹ were found in the U-containing lepidocrocite spectrum, indicating that the lepidocrocite structure was maintained after coprecipitation. GR II reduced the uranium upon coprecipitation; therefore, only a small peak was observed at 920 cm⁻¹, which may indicate some reoxidation of uranium in air during analysis. Interestingly, the U-containing ferrihydrite exhibited a broader peak at 900 cm⁻¹, which may be caused by either (i) an increased energy difference between the O=U=O asymmetric stretching and μ -OH bending component peaks or (ii) the amorphous nature of the coprecipitate. The stretching frequencies for the ferrihydrite and lepidocrocite samples may be influenced by coordination with iron. Allen et al. (29) observed that the trend to greater average distances for uranyl ion in the oxides should be reflected by shifts in the uranyl absorption band to lower energy. The trend in our data in general confirm this observation, except for the maghemite stretching frequency, which is shifted to higher energy. This peak is very broad and may contain a strong μ -OH component in addition to uranyl stretching.

Discussion

The oxides commonly associated with corroded steel surfaces include ferrihydrite, goethite, GR II, lepidocrocite, maghemite, and magnetite. The association of uranium with the oxide is dependent on the nature of the oxide. Addition of uranyl ion to iron oxides resulted in its attachment to surface sites

as an inner-sphere bidentate complex (10, 11). The addition of uranium during coprecipitation with iron may result in bi- and tri-dentate bonding with iron, formation of di- and tri-nuclear Fe-U complexes, and polymeric forms of uranium oxyhydroxide. During the crystallization process, the uranium may also become encapsulated into the oxide as a microcrystalline phase (30).

We compared the association of uranium coprecipitated with ferrihydrite to an aged ferrihydrite (10). Although the formation of a bidentate inner-sphere complex with iron is confirmed in both forms, there are distinct differences in the 2 O atoms in the U-O_{eq2} shell. A smaller Debye-Waller factor (an indication of the thermal and static disorder in the atomic shell) for the coprecipitate (0.0050) as compared to the aged form (0.0084) suggests that the U-O sites are more uniformly distributed during coprecipitation.

Coprecipitation of uranium with goethite resulted in the formation of an oxyhydroxide species. The coprecipitation of the uranium-mineral under alkaline conditions (pH 12) may have been a contributing factor to its formation. Misawa et al. (6) noted that goethite may also be formed under acidic conditions. No uranium association with the crystalline goethite as an inner-sphere complex was indicated as reported by Moyes et al. (11). Lepidocrocite exhibited an inner-sphere bidentate coordination of uranium with iron, similar to that for ferrihydrite.

The coprecipitation of uranium with maghemite or magnetite resulted in the formation of uranium hydroxide or oxyhydroxide species. The absence of U-Fe interactions indicates that uranium is most probably found in microcrystalline form on the oxide surface. The dissolution pattern of the uranium by dilute HCl supports this interpretation.

The observed XPS binding energies for goethite, maghemite, and magnetite are correlated with the number and radial distances of first equatorial shell O atoms. There are 2.8 O atoms at a distance of 2.26 Å in the first shell for goethite and 1.5 and 1.6 O atoms, respectively, for maghemite and magnetite. The resulting higher ionic character of the U-O bond leads to slightly higher core electron-binding energies. The broadness of the U4f photoelectron peaks indicates that these are multiplets containing narrower peaks corresponding to the various O atoms in different coordination with U. Not enough information, however, is available to allow for deconvolution of any close singlets in the peak envelope, but an increase in the ionicity of particular bonds contributing to the multiplet would result in the observed shift (23). The presence of a Fe-U interaction for the lepidocrocite and ferrihydrite makes a similar comparison difficult. The uranium in GR II exhibited a binding energy of 380.9 eV, similar to that observed for uranium dioxide (380.4 eV), suggesting that uranium is in the tetravalent state. No peak for hexavalent uranium was noted. Analysis of the sample oxides at the Fe2p binding energy shows the Fe to be bonded primarily to hydroxyl groups and as Fe₂O₃ (data not shown).

The synthesis of GR II in the presence of U resulted in its reduction to tetravalent form with the formation of magnetite. The stoichiometric decrease in the ratio of Fe(II):total Fe from 0.73 in the absence of uranium to 0.62 confirms the role of ferrous ion in the reduction of uranium. Liger et al. (31) have shown that reduction of uranium occurs on suspensions of hematite in the presence of ferrous ion surface complexes $\equiv\text{FeOFe}^+$ and $\equiv\text{FeOFeOH}^0$ at alkaline pH. It was postulated that the surface complex provided a favorable coordination environment for electron transfer from iron to uranium. Brooks and co-workers (32) observed that electric field-induced deprotonation of GR II hydroxyl groups resulted in charge redistribution from univalent hydroxyl oxygen to divalent oxygen with oxidation of ferrous to ferric ion. This resulted in formation of lepidocrocite or goethite; similarly, deprotonation of green rust I resulted in akaganeite

(β -FeOOH) formation. The presence of cations and anions are also known to affect the formation of iron oxides. Ishikawa et al. (33) demonstrated that addition of Co(II) and Cu(II) during the synthesis of Fe(OH)₂ resulted in production of magnetite and inhibited goethite crystallization while the presence of Cr(III) exhibited the opposite effect. Using X-ray diffraction analysis, Refait et al. (34) established that the structure for a synthetically prepared green rust I consisted of Fe(OH)₂ sheets alternating regularly with negatively charged interlayers of chloride ions and water molecules.

The rate and extent of uranium dissolution from the various oxides was dependent upon its association. Uranium associated as oxyhydroxide species with goethite, maghemite, and magnetite underwent rapid dissolution followed by a slow dissolution of iron. This was predominantly due to the association of uranium with the oxide surface. Uranium formed an inner-sphere bidentate complex with iron in ferrihydrite and lepidocrocite, and we observed concomitant dissolution of the uranium and iron. The mechanism of uranium dissolution from GR II could not be established because of the complexity of the oxide phase. However, its rapid dissolution in dilute acid as compared to the iron indicates that it is probably present as a uranous oxyhydroxide species. These results suggest that an understanding of the nature of the radionuclide association with various oxides formed on corroding steel surfaces may aid in the development of appropriate decontamination technology.

Acknowledgments

We acknowledge the technical assistance of Alex Schill in preparing the green rust. This research was performed under the auspices of the Environmental Management Science Program (EMSP), Decontamination and Decommissioning Focus Area, Office of Science and Office of Environmental Management, U.S. Department of Energy, under Contract DE-AC02-98CH10886.

Literature Cited

- (1) Buckentin, J. M.; Damkroger, B. K.; Schlienger, M. E. *Radioactive Scrap Metal Decontamination Technology Assessment Report*; SAND96-0902; Sandia National Laboratories: Albuquerque, NM, 1996; p 9.
- (2) Oh, S. J.; Cook, D. C.; Townsend, H. E. *Corros. Sci.* **1999**, *41*, 1687.
- (3) Wolski, W. *Science* **1990**, *46*, 743.
- (4) McGill, I. R.; McEnaney, B.; Smith, D. C. *Nature* **1976**, *259*, 200.
- (5) Music, S.; Gotic, M.; Popovic, S. *J. Mater. Sci.* **1993**, *28*, 5744.
- (6) Misawa, T.; Hashimoto, K.; Suetaka, W.; Shimodaira, S. In *Proceedings of the Fifth International Congress on Metallic Corrosion*, Tokyo, Japan, May 1972; NACE: Houston, TX, 1974; p 775.
- (7) Gabriel, U.; Gaudet, J.-P.; Spadini, L.; Charlet, L. *Chem. Geol.* **1998**, *151*, 107.
- (8) Sato, T.; Murakami, T.; Yanase, N.; Isobe, H.; Payne, T. E.; Airey, P. L. *Environ. Sci. Technol.* **1997**, *31*, 2854.
- (9) Bruno, J.; dePablo, J.; Duro, L.; Figuerola, E. *Geochim. Cosmochim. Acta* **1995**, *59*, 4113.
- (10) Waite, T. D.; Davis, J. A.; Payne, T. E.; Waychunas, G. A.; Xu, N. *Geochim. Cosmochim. Acta* **1994**, *58*, 5465.
- (11) Moyes, L. N.; Parkman, R. H.; Charnock, J. M.; Vaughan, D. J.; Livens, F. R.; Hughes, C. R.; Braithwaite, A. *Environ. Sci. Technol.* **2000**, *34*, 1062.
- (12) Bargar, J. R.; Reitmeyer, R.; Lenhart, J. J.; Davis, J. A. *Geochim. Cosmochim. Acta* **2000**, *64* (16), 2737.
- (13) Raven, K. P.; Jain, A.; Loeppert, R. H. *Environ. Sci. Technol.* **1998**, *32*, 344.
- (14) Atkinson, R. J.; Posner, A. M.; Quirk, J. P. *J. Phys. Chem.* **1967**, *71*, 550.
- (15) Srinivasan, R.; Lin, R.; Spicer, R. L.; Davis, B. H. *Colloids Surf.* **1996**, *113*, 97.
- (16) Schwertmann, U.; Cornell, R. M. In *Iron Oxides in the Laboratory: Preparation and Characterization*; VCH Publishers: New York, 1991.

- (17) Cornell, R. M.; Schwertmann, U. *The Iron Oxides: Structure, Reactions, Occurrence and Uses*; VCH Publishers: New York, 1996; p 494.
- (18) Sidhu, P. S.; Gilkes, R. J.; Posner, A. M. *J. Inorg. Nucl. Chem.* **1978**, *40*, 429.
- (19) *Standard Methods for the Examination of Water and Wastewater*, 19th ed.; American Public Health Association (APHA): Washington, DC, 1995.
- (20) Johnson, D. A.; Florence, T. M. *Anal. Chim. Acta* **1971**, *53*, 73.
- (21) Zabinsky, S. I.; Rehr, J. J.; Ankudinov, A.; Albers, R. C.; Eller, M. *J. Phys. Rev. B: Solid State* **1995**, *52*, 2995.
- (22) Savitsky; Golay, M. J. E. *Anal. Chem.* **1964**, *36*, 8.
- (23) Sherwood, P. M. A. In *Practical Surface Analysis*; Briggs, D., Seah, M. P., Eds.; John Wiley and Sons: New York, 1983; p 445.
- (24) Halada, G. P.; Clayton, C. R. *J. Vac. Sci. Technol., A* **1993**, *11*, 2342.
- (25) Halada, G. P.; Kim, D.; Clayton, C. R. *Corrosion* **1996**, *52*, 36.
- (26) Hudson, E. A.; Allen, P. G.; Terminello, L. J.; Denecke, M. A.; Reich, T. *Phys. Rev. B: Condens. Matter* **1996**, *54*, 156.
- (27) Francis, A. J.; Dodge, C. J.; Gillow, J. B.; Papenguth, H. W. *Environ. Sci. Technol.* **2000**, *34*, 2311.
- (28) Veal, B. W.; Lam, D. J.; Carnall, W. T.; Hoekstra, H. R. *Phys. Rev. B: Condens. Matter* **1975**, *12*, 5651.
- (29) Allen, P. G.; Shuh, D. K.; Bucher, J. J.; Edelstein, N. M.; Palmer, C. E. A.; Silva, R. J.; Nguyen, S. N.; Marquez, L. N.; Hudson, E. A. *Radiochim. Acta* **1996**, *75*, 49.
- (30) Ohnuki, T.; Isobe, H.; Yanase, N.; Nagano, T.; Sakamoto, Y.; Sekine, K. *J. Nucl. Sci. Technol.* **1997**, *34*, 1153.
- (31) Liger, E.; L. Charlet; P. van Cappellen. *Geochim. Cosmochim. Acta* **1999**, *63*, 2939.
- (32) Brooks, A. R.; Clayton, C. R.; Doss, K.; Lu, Y. C. *J. Electrochem. Soc.* **1986**, *133*, 2459.
- (33) Ishikawa, T.; Nakazaki, H.; Yasukawa, A.; Kandori, K.; Seto, M. *Corros. Sci.* **1999**, *41*, 1665.
- (34) Refait, P.; Abdelmoula, M.; Genin, J.-M. R. *Corros. Sci.* **1998**, *40*, 1547.

Received for review November 30, 2001. Revised manuscript received May 28, 2002. Accepted May 28, 2002.

ES011450+